

3D Master-based Method for Optimizing the Cost Calculation of PBF-LB/M Manufactured Parts

Briac Lanfant, Silvan Lack, Benjamin Meyer, Ahmed Abdulkadir, Thilo Stadelmann,
Daniel Schmid

ZHAW Zurich University of Applied Sciences, Switzerland

Corresponding author:

Dr. Briac Lanfant

ZHAW School of Engineering

Lagerplatz 22

8400 Winterthur, Switzerland

briac.lanfant@zhaw.ch

Received: 19 December 2024; accepted:

ABSTRACT

The 3D Master method streamlines the transfer of product information from design to production, utilizing 3D model files containing Product Manufacturing Information. This approach facilitates direct access to crucial data like materials, geometric dimensions, and tolerances for each step of the metal additive manufacturing (MAM) of parts. By leveraging this data, the 3D Master method enables the automation of accurate cost evaluation.

This contribution introduces a method leveraging the 3D Master to automate a precise manufacturing cost calculation for MAM parts using powder-based fusion processes. It proposes a frame based on the quality level of the data provided by the customer to quantify the accuracy of the estimated cost, thanks to a performance index (KPI). A build cost model based on an optimal volumetric energy density calculation achieved through a theoretical and statistical approach is also provided. The study, conducted on 20 reference MAM parts of varying geometrical complexities, demonstrates a relative deviation of normalized actual and calculated cost difference below 10 %.

This cost model and the KPI give solid foundations for a service provider to assess the production cost at the early stages of the production process and lay the groundwork for a commercial online service platform offering reliable and adapted quotes for MAM part production within minutes.

KEYWORDS

3D Master approach; PMI; Customer technical interface; Manufacturing service provider; 3D printing; PBF-LB/M, Cost model; AI-based PMI mapping

3D Master-basierte Methode zur Optimierung der Kostenkalkulation von PBF-LB/M-Fertigteilen

ABSTRACT

Die 3D Master Methode rationalisiert die Übertragung von Produktinformationen vom Entwurf bis zur Produktion, indem 3D-Modelldateien mit Produktherstellungsinformationen verwendet werden. Dieser Ansatz erleichtert den direkten Zugriff auf wichtige Daten, wie Materialien, geometrische Abmessungen und Toleranzen, für jeden Schritt der additiven Metallfertigung (MAM) von Teilen. Durch die Nutzung dieser Daten ermöglicht die 3D Master Methode die Automatisierung einer genauen Kostenberechnung. In diesem Beitrag wird eine Methode vorgestellt, die den 3D Master nutzt, um eine präzise Berechnung

der Herstellungskosten für MAM-Teile mit pulverbasierten Fusionsverfahren zu automatisieren. Es wird ein Rahmen vorgeschlagen, der auf dem Qualitätsniveau der vom Kunden bereitgestellten Daten basiert, um die Genauigkeit der geschätzten Kosten dank eines Leistungsindex (KPI) zu quantifizieren. Ein Baukostenmodell, das auf einer optimalen Berechnung der volumetrischen Energiedichte basiert, die durch einen theoretischen und statistischen Ansatz erreicht wurde, wird ebenfalls vorgestellt. Die Studie, die an 20 MAM-Referenzteilen unterschiedlicher geometrischer Komplexität durchgeführt wurde, zeigt eine relative Abweichung der normierten tatsächlichen und berechneten Kosten unter 10 %.

Dieses Kostenmodell und der KPI bilden eine solide Grundlage für einen Dienstleister zur Bewertung der Produktionskosten in den frühen Phasen des Produktionsprozesses und legen den Grundstein für eine kommerzielle Online-Serviceplattform, die innerhalb von Minuten zuverlässige und angepasste Angebote für die Produktion von MAM-Teilen bietet.

SCHLÜSSELWÖRTER

3D-Master-Ansatz; PMI; Technische Kundenschnittstelle; Fertigungsdienstleister; 3D-Druck; PBF-LB/M, Kostenmodell; KI-basiertes PMI-Mapping

1.Introduction

Facing higher demands for non-standard products, enterprises are transforming every step of the production process to be more flexible and efficient, notably by incorporating smart solutions brought together under the concept of Industry 4.0. The integration of 3D printing technologies, especially powder-based fusion (PBF) processes [1, 2], belongs to the adaptive strategy of the production sector toward mass customized production as they enable the manufacturing of products with peculiar shapes and innovative functionalities [3, 4].

Along with these transformations, the producers and service providers have to modify their customer's technical interfaces. These interfaces, dedicated to collect product specifications from customers and to provide a price and delivery time, must remain fast and accurate even for new and unique products such as 3D printed parts.

However, the current approach of collecting data with such interfaces causes a breakup of the product lifecycle's digital thread. Indeed, only 3D models and some details, like product material, printing technology, and eventually a 2D drawing and post-processing, are usually requested. This transfer induces a loss of production information and can give room to misinterpretations, often resulting in the need for direct clarifications between the producer and customer. The purpose of a fast service providing accurate prices is thus rendered ineffective.

This contribution gives a frame based on the 3D Master approach to evaluate the incertitude caused by the quality level of data collected for Metal Additive Manufactured Parts (MAM) when a production cost is assessed. We also show how the Product Manufacturing Information (PMI) can be exploited to quicken a safer data transfer process from customer to producer while bringing a solid foundation for an accurate cost calculation.

3D Models, PMI, and 3D Master Approach

The conventional approach to print parts is based on the 3D model and additional requirements for the postprocessing. The 3D model, which includes the part's shape, dimensions, and features, is needed to generate the laser paths for each layer in the printing process (see Fig. 1, model of the raw part). Post-processing is necessary, at least for removing support structures [5]. More frequently, post processing addresses other critical functional and aesthetic requirements such as tolerances, holes and

threads, surface finishes, and additional specifications detailed in a manufacturing 2D drawing (see Fig. 1, model and drawing of finished part).

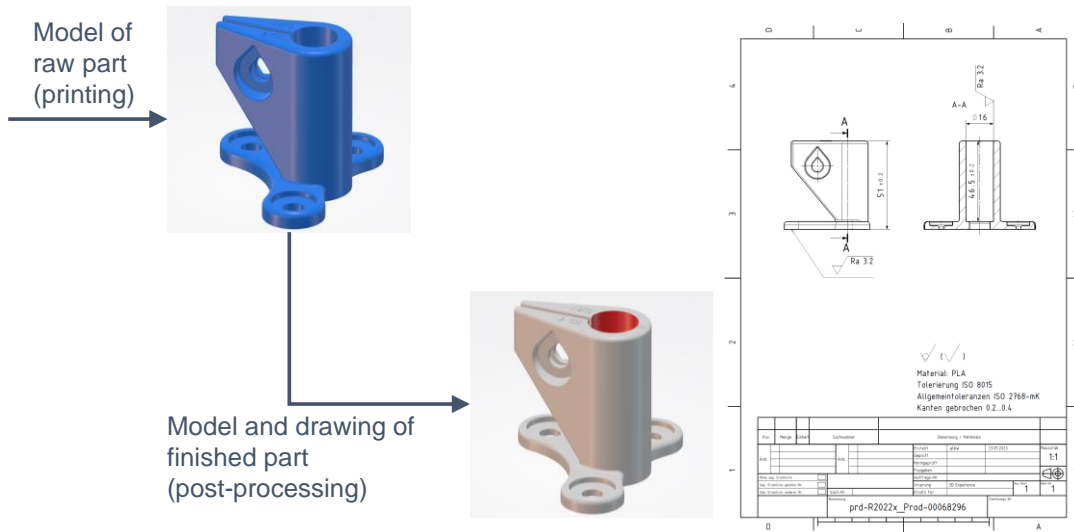


Fig. 1: Conventional approach including a drawing of the finished part

The combination of the 3D model and the manufacturing 2D drawing is a well-established practice, particularly in part machining. The 2D drawing serves as a guide for machinists, ensuring that the part is manufactured following the precise specifications, and acts as the definitive source of truth, having been validated by the responsible product manager. The approval and version information are typically embedded electronically in the drawing from the company's Enterprise Resource Planning (ERP) system.

However, this traditional approach has its limitations. It can be time-consuming and prone to errors, especially when complex geometries are involved. Additionally, any changes in the design require updates to both the 3D model and the manufacturing drawing, which can lead to inconsistencies if not managed properly. Therefore, state-of-the-art computer-aided design (CAD) software offers the opportunity to merge models and drawings [6]. With this approach, the product manufacturing information (PMI) [7] is no longer documented on the manufacturing drawing but is a part of the 3D model. Moreover, PMI, which includes critical tolerances, material, surface finish requirements, and other manufacturing instructions, such as metadata (lifecycle state and creation date for example), is no longer solely documented on the manufacturing drawing. The data is ideally machine-readable and is processable by subsequent software tools, e.g., computer-aided manufacturing (CAM). A drawing-free workflow is created [6].

Related software platforms (for example [8, 9] [10]) offer today the interoperability of software packages. Therefore, CAD objects can be handled by the compatible CAM and PMI can be processed by the CAM Designer. Company-internal processes and the Product Lifecycle Management (PLM) and ERP systems handle the correct versioning and maturity state, even when different software tools are used.

However, depending on the Make or Buy strategy of companies, the manufacturing of parts might be outsourced. When these companies do not provide direct access to the CAD/PLM system to their suppliers, one of the best-known standards for exchanging information between platforms and software is STEP (STandard for the Exchange of Product model data, ISO 10303) [11]. Today, this standard partly covers PMI [12], although the use of PMI is not yet common in the industry [13] (statement based on additive manufacturing parts).

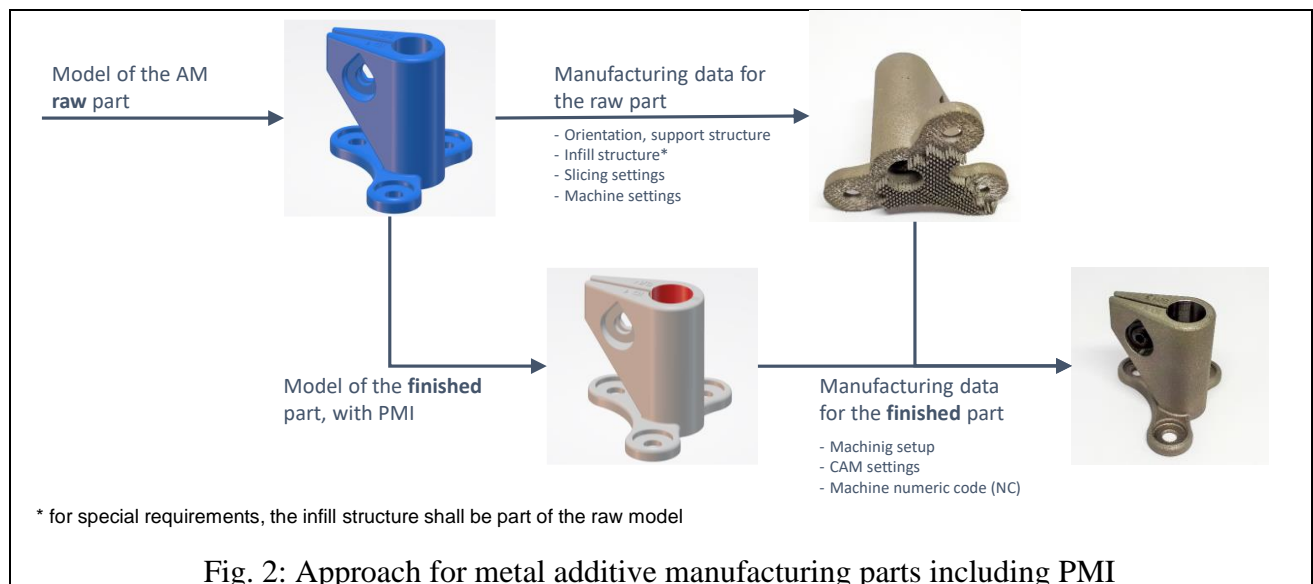
Suppliers specializing in prototypes and contract manufacturing are typically using the STEP's strength to offer related web-based services, where manufacturing data are collected via customer technical interfaces. For example, with [14], a STEP file is uploaded, additional information about

the part needs to be selected or stated, and a price and delivery time are given within due time. Optionally, the related 2D drawing can be uploaded and consulted for manufacturing reasons after the pricing and order release. For these service providers, and especially for those using automated ordering processes via service platforms, four challenges predominate.

- Most of the uploaded STEP files do not include PMI, therefore automated manufacturing cost calculation is difficult and unprecise.
- Tools (e.g. [15]) for cost calculation are typically not interpreting PMI.
- STEP format, as such, covers PMI in a semantic and non-semantic way, therefore geometric dimensioning and tolerancing (GD&T) interpretation is incomplete or a related interpreter needs to be established.
- Material and Metadata, like the revision number or lifecycle state, are not standardized and need to be added as text notes to one or more pre-defined views of the part.

In such a case, a manufacturing service provider should ideally handle data following the 3D Master approach [6, 11]. The 3D Master approach enables the enhancement of the data provided by the designer (particularly the 3D model with PMI) by incorporating data from the manufacturer, resulting in a comprehensive data set that contains all the necessary information. This approach links together the following data: the STEP file (ideally including PMI), the drawing, the complete commercial offer, and the manufacturing machine code (Computer Numerical Control, CNC) along with the machine information. The aim is to keep a record of the entire job so that it can be, if needed, immediately re-executed from the same data set.

In the context of metal additive manufacturing, effective data handling is of the highest importance (see Fig. 2 and [13]). For example, it is essential to have not only the model of the final additive manufactured part with PMI but also the model of the raw part related to the printing step as the difference between the raw and final parts, called allowance [16], determines the final machining requirements. Such a raw-final models' approach is well-established in the casting community.



In fact, the product data quality varies depending on the AM expertise of the client. Poor data quality reduces the accuracy of the production cost calculation and can induce extra production costs. Therefore, a service provider needs to anticipate extra production costs due to lacking information when giving its customer a price through the service platform.

In this work, we propose to give a frame based on the quality level of the data provided by the customer to quantify the accuracy of the estimated cost, thanks to a performance index (KPI - see Section 2.1). This performance index could support the service provider to add a safe and appropriate margin covering unexpected costs.

Cost Models for MAM by Power Bed Fusion (PBF)

Cost modeling of additively manufactured parts has been extensively researched during the last 20 years. The works of [17–20] especially have given the main foundation for establishing the cost equations of 3D printing processes. These models gained accuracy and precision during the last decade thanks to research studies investing more effort in peculiar details, such as specific 3D technologies [1, 21], specific cost drivers such as design [22, 23], or energy [24, 25], or dedicated applications [24, 26–29].

Among the different approaches classified by Kadir et al. in [21], the process-based method has been the most used by researchers. Due to its analytical trait, this method aims to provide an exhaustive and detailed description of all cost elements, which results in a cost estimation close to the real cases.

Process-based cost equations for PBF are generally divided into three main components:

- C_{prep} , the *cost of preparation operations*, such as data preparation, material preparation, or setup of the printing machine.
- C_{build} , the *build cost*, encompasses expenses directly related to the 3D parts printing step. It usually includes the material cost as well as the cost of the machine in operation. The operator's cost might also be considered when human supervision is needed during the printing.
- C_{post} , the *Post-processing cost*. This last category comprises all the costs related to steps needed after the printing, such as the removal of powder, the heat treatment, the separation from the build plate, the removal of the support structures, the CNC machining, and surface finishing. Costs related to quality control belong to this category.

Analytical models to effectively calculate the final cost imply a perfect understanding and control of the entire production process, which involves the examination of numerous parameters as well as their interactions. The powder quality effect [30], the planning of a batch with different geometries [18, 31], the ill-structured cost [29, 32, 33], or the consideration of the life cycle cost effect on the hourly rate of production machines, for example, are only some aspects to be evaluated.

Therefore, cost evaluation at early stages of the production, as it is the case for a customer technical interface of service web platforms, is arduous [34], especially because 3D parts are often unique and produced only once.

Moreover, the high amount of required data is difficult to gather. From more than 50 reviewed scientific papers related to the cost of metallic parts printed with a laser-based PBF (PBF-LB/M) process, only a few could obtain real production information from companies and confront their cost models with concrete cases [26, 29, 35].

Despite different cost model approaches, most works agree that the build cost, C_{build} , greatly contributes to the total cost of a printed part [34]. According to [26, 36–38], C_{build} weighs from 50 to 70% of the total cost and must be therefore considered carefully.

However, 75% of reviewed papers on the related topic do not explain how to calculate the C_{build} - more specifically the build time t_{build} . Only 8% provide quantitative information on the parameters used, but no justification is mentioned regarding their selection. This lack of documentation can be notably explained by the fact that t_{build} is directly related to parameters critical for the quality of a MAM product: as a part of their core know-how, producers are mostly reluctant to publish them.

Acknowledging the complexity of using analytical models and the lack of data to evaluate the cost of MAM parts, we focus in Section 2.2 on a model to assess build costs that can be effectively used

when PMI, 3D Models, and drawings are typically the only information available. This model can provide solid foundations for the service provider to assess the production cost at the early stages of the production process.

2. Method

2.1 Combined Flow Model for Raw and Finished Part

2.1.1 Data Flow

As mentioned in Section 1, manufacturing 3D metallic parts requires ideally two models, one for the raw (printed) part and one for the final part. The complexity of additive manufacturing emphasizes the importance of release processes and the related data handling. Considering the 3D Master approach, it is recommended to store and release the following information in the PLM system to enable the reproducibility of a part manufacturing job.

1. The raw model for the additive manufacturing part.
2. The printing definition (e.g. orientation, support structures, internal structure, and slicing).
3. The model for the final part including PMI.
4. The final machining (including e.g. production means, sequence, tools, and CNC code).


Further files are needed for the manufacturing process. However, they are directly generated from the above-mentioned elements, so storing and releasing them is not mandatory. For example, STL (acronym for stereolithography [39]) files are directly exported for the raw model and are thus reproducible.

In the case of a manufacturing service provider [14], the request for quotation starts with list items 1 and 3 considering that no printing and machining has ever been done before with this part. Due to the lack of interoperability, there are no native models available but STEP files. Therefore, the 3D Master approach needs to be adapted and STEP files are the related starting point. The printing definition and the final machining (list items 2 and 4) are added accordingly after the first manufacturing job. As shown by a survey in [13], the industry has not yet adopted this way of working. Therefore, the manufacturing service provider has to enable its service platform to handle different types of data and combinations of input, e.g. a pure final AM model without PMI.

2.1.2 Impact on Cost Calculation and Pricing

To assess the different combinations of the data set, we propose to define a Formal Quality Level (FQL) that attributes a degree of expertise to the customer depending on the provided information (Table 1).

Table 1: Formal Quality Level of uploaded data for MAM parts

FQL	Expert							Beginner
	8	7	6	5	4	3	2	1
Model of the final part with PMI	X	X				X		
Model of the final part			X	X	X		X	X
Drawing of the final part	X		X	X			X	
Model of the raw part with PMI	X	X						
Model of the raw part			X	X	X			

Drawing of the raw part	X	X
-------------------------	---	---

At least eight levels can be identified. Further combinations of uploaded files are possible but not given here for sake of simplicity. FQL 7 and 8 represent the highest standard of data combination, while FQL 1 is the lowest configuration that can be expected for a manufacturing service provider [14]. The lower the FQL, especially level 3 and less, the more the AM part manufacturer will have to provide effort because the model of the raw part must be established. Without this information, the final machining cannot be defined from the volume difference between the raw and final part, and the post- processing cost C_{post} cannot be formally calculated.

FQL 8 specifically raises the issue related to the STEP format. Even with PMI, associated metadata cannot be exported with STEP files. In this regard, a drawing containing these inputs might be required. Specific algorithms (optical character recognition (OCR), artificial intelligence (AI), or similar) could automatize the metadata recognition. Assuming a mature AI technology capable of feature interpretation (see section 2.3), it is currently unknown which FQL among the levels 6, 7, or 8, would be preferable for a manufacturing service provider.

To quantify the variation in cost calculation depending on the FQL, an adapted standard deviation based on the normalized (with the actual costs as reference) cost (C) difference between estimated (C_E) and actual (C_A) costs is taken as the key performance index (KPI).

$$KPI_{Level\ x} = \sqrt{\frac{\sum_{i=1}^n \left(\frac{C_{E,i} - C_{A,i}}{C_{A,i}} \right)^2}{n - 1}} \quad (1)$$

The lower the KPI the better the general cost assessment is. High formal quality levels (typically levels with PMI) are expected to give low KPIs, while lower FQLs should induce higher values of this index.

Assuming this trend, the KPI can be a relevant criterion to establish “safety margins” during the pricing on the manufacturing service provider’s commercial platform, in order to provide a customer with an accurate price even for low FQL. Low KPIs should lead to low safety margins, and higher performance indexes should induce higher margins to cover the cost incertitude caused by the lack of data.

2.2 Build Cost Model for MAM Parts

According to the build cost description defined in Section 1, the build cost per part i is:

$$C_{Ebuild,i} = V_i * \rho_i * C_{mat,i} + t_{build,i} * C_{Machine\ H.rate} \quad (2)$$

V_i is the volume of the raw (printed) part, ρ_i the material density, and $C_{mat,i}$ the material cost per kg. $t_{build,i}$ is the time needed to print the part i and $C_{machine\ H.rate}$ is the machine hourly rate.

V_i and ρ_i are provided from the PMI, while $C_{mat,i}$ and $C_{machine\ H.rate}$ can be collected from the market.

The build time $t_{build,i}$ consists of the following terms:

- $\sum_i t_{scan,i}$: sum of the times $t_{scan,i}$, where $t_{scan,i}$ is the time needed to scan a part i
- $\sum_i t_{scan.structure,i}$: sum of the times $t_{scan,structure,i}$, where $t_{scan,structure,i}$ is the time needed to scan the support structure of a part i
- $t_{coating}$: time needed for spreading layer by layer the powder bed

- t_{delay} : time needed for the laser(s) to cross unmelted areas

For the following, we assume a continuous laser with a constant laser spot diameter d . Scan speed variations are regarded as neglectable. Finally, keeping in mind that the post-processing includes CNC machining and surface finishing, no contour is needed for surface quality improvement of the printed part.

2.2.1 Calculation of $t_{scan,i}$

For a part i , the $t_{scan,i}$ is comprehended as the total scan length of the laser, $L_{scan,i}$, divided by the laser scan speed u_{las}

$$t_{scan,i} = \frac{L_{scan,i}}{u_{las}} \quad (3)$$

Independently from the shape of the raw part i , its volume V_i can be expressed as:

$$V_i = h_{max,i} * S_i \quad (4)$$

where $h_{max,i}$ is the maximum height of a part i ideally oriented for the printing, and S_i is the related surface.

Considering d_{over} , the overlapping of the laser paths, and d the diameter of the j lasers, the total laser path $L_{scanS,i}$, for the surface S_i is:

$$L_{scanS,i} = \frac{S_i}{(1 - d_{over}) * d * j} \quad (5)$$

Defining η as the hatch distance, equation (5) can be comprehensively turned into:

$$L_{scanS,i} = \frac{S_i}{\eta * j} \quad (6)$$

The term $h_{max,i}$, can be further expressed with n_i the total number of layers of the part i , and h the height of one layer:

$$h_{max,i} = n_i * h \quad (7)$$

From equations (4), (6) and (7), V_i is therefore developed as:

$$V_i = n_i * h * L_{scanS,i} * \eta * j \quad (8)$$

The total scan length of the laser $L_{scan,i}$ been the total number of layer n_i multiplied by $L_{scanS,i}$, the equation (9) is finally written:

$$L_{scan,i} = \frac{V_i}{\eta * h * j} \quad (9)$$

With (3) and (9), $t_{scan,i}$ can be evaluated with the V_i volume of the raw part, three printing parameters (η , h and u_{las}), and j the number of lasers:

$$t_{scan,i} = \frac{V_i}{\eta * h * u_{las} * j} \quad (10)$$

Thus, the scan time $t_{scan,i}$ is shown to depend on only a few parameters: V_i , η , h , u_{las} and j . Among the data available in PMI following a 3D master approach, only V_i is directly provided (starting FQL4). No information is given about η , h , and u_{las} , which are, as mentioned further above (section 1), usually not shared by producers due to their criticality. The number of lasers j can be provided by the producer or machine supplier.

Nevertheless, information such as material and roughness can address the problem of restricted access to η , h , and u_{las} : we show below that a theoretical approach to a process map and a statistical consideration of the volumetric Energy Density (ED) can lead to a relevant identification of these parameters.

To the best of the author's knowledge, the relationship between the scan time t_{scan} , the material properties and ED has never been presented before in the field of the cost modeling of MAM parts printed with a PBF-LB process.

Identification of h , u_{las} and η :

If AM processes are usually more expensive than traditional processes like milling or injection molding, their potential of producing complex and light shapes gives them a prior advantage. Lightweight products with unique shapes that reduce the assembly steps are especially attractive for transport applications. The high-quality standards in this sector require producers to print parts with high material density, as a necessary condition to guarantee that theoretical properties are reached. Process parameters for MAM parts have thus to be primarily selected to ensure high printing quality. Lowering the cost, and therefore the processing time, comes second in priority but is still important regarding both customer (affordability) and producer (competitiveness).

Relying on a process map with u_{las} and the laser power P as variables, (see Fig. 3 as an example), four main density related structure areas of a printed product can be identified:

- The dense area (DA) is associated with parts reaching densities generally above 99.0% and thus showing, for a given microstructure, material properties close to theory. Printing conditions linked to this area enable the development of a stable melt pool in a thermal conduction mode [40].
- Keyhole (KH) are typically rounded pores appearing when the energy density in the material exceeds a threshold value, above which strong evaporation and high melt pool dynamics occur. A complex combination of physic phenomena such as vapor shielding, gas recoil, Marangoni convection and multi-reflections induce the formation of deep keyhole depressions.
- Balling (BL) can be associated with two types of events [41]. The balling of type I (BLI) is related to high surface tensions and insufficient liquid and leads to a poorly wet and discontinuous melt track. The Balling of type II ($BLII$) is regarded as projections of micrometric metal drops.
- Lack of Fusion (LoF) happens when energy delivered during the printing process is not sufficient to melt the powder bed and/or merge the molten tracks together. LoF pores are characterized by an undefined shape and are specifically located between layers or tracks

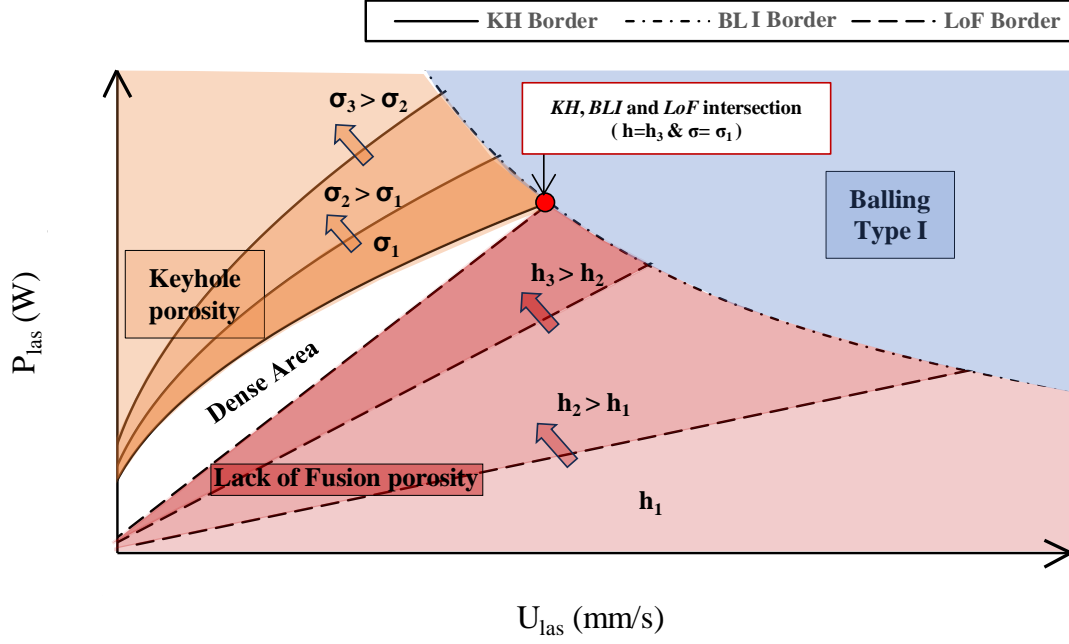


Fig. 3: Process map with P - u_{las} space

Considering the P - u_{las} space, the producers of MAM parts must select process parameters corresponding to the DA . The borders of the dense area DA can be delimited thanks to a combination of restrictive conditions based on melt pool dimensions (Fig. 4) and analytical models, as described in the following paragraphs:

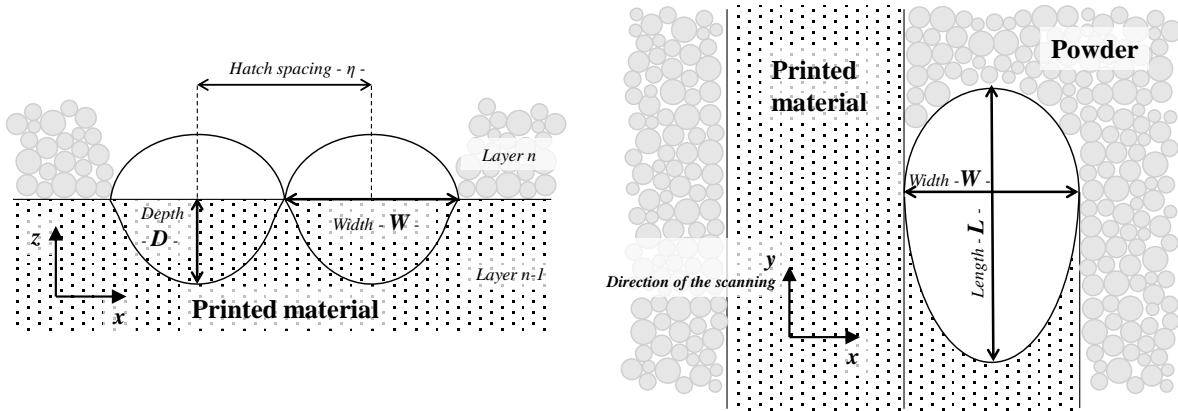


Fig. 4: Melt pool dimensions

KH border definition: Seede et al. [42] and Oliveira et al. [43] have recently referred to the analytical E-T model [44] to evaluate the dimensions of the melt pool near the transition $DA \rightarrow KH$. However, if this model is satisfying in the conduction mode, it needs corrections and calibration to provide accurate dimensions. It is moreover not a relevant model to evaluate the melt pool shape for printing conditions close to KH domain, because it neglects phenomena such as Marangoni convection and recoil pressure. Zhu et al. [41] observe that the G-S model provides theoretical values closer to the measured dimensions. This model could be used with precaution to compute melt pool dimensions in the $DA \rightarrow KH$ border vicinity.

According to [42] and [43] the limit $DA \rightarrow KH$ can be defined with a geometrical criterion. A ratio Depth over Width (D/W , see Fig. 4) ranging from 1.2 to 1.5, at least above 1, indicates the Keyhole mode. Beyond imprecisions caused by the melt pool measurements, Cunningham et al. [45] show that

keyhole-like vapor depression, which can presumably already induce KH pores, occurs before the change of the shape of the melt pool to a D/W ratio superior to 1.

A more conservative approach is given in the work of King et al. [40]: by taking into account the role of the vapor recoil pressure and surface tension of the molten metal, they establish that the $DA \rightarrow KH$ border is reached when the normalized enthalpy $\Delta H/H_s$ is superior to the ratio $\frac{\pi * T_b}{T_m}$:

$$\frac{\Delta H}{h_s} = \frac{A * P}{\pi * h_s * \sqrt{\alpha * u_{las} * \sigma^3}} > \frac{\pi * T_b}{T_m} \quad (11)$$

Where ΔH is the specific enthalpy, h_s is the product of the density of the material with the heat capacity and the melting temperature, and A is the absorptivity. α is the thermal diffusivity of the molten material, and σ the laser spot size. T_b and T_m are respectively the boiling and melting temperature of the printed material.

Therefore, apart from the two process variables P and u_{las} , the $DA \rightarrow KH$ border depends on σ (illustration in Fig. 3) and on the printed material. The laser spot size σ can be obtained without hurdle, while the material and its properties are provided by the PMI and materials handbooks.

BL border definition: While the balling of type II mostly happens in the KH area due to high and fluctuating vapor depressions near the melt pool, the balling area shown in Fig. 3 refers to BLI . Necessary conditions for the $DA \rightarrow BLI$ transfer are based on more established geometrical criteria, as notably reminded in [41]:

$$\frac{\pi W}{L} > \sqrt{\frac{2}{3}} \quad (12)$$

If the E-T or G-S models can provide the melt pool dimensions, the calculation of the melt pool length L is practically difficult to validate with ex-situ measurements and is therefore unreliable. It leads, for example, Zhu et al. to use a correction factor to adjust it. Nevertheless, the work in [46] mentions that the ratio of L/W can be expressed solely with the variables P and u_{las} , the Euler's number e , and the material properties (where k is the thermal conductivity – T is set at the temperature of interest T_m), as shown in equation (13)

$$\left(\frac{L}{W}\right)^2 = \frac{A * e * P * u_{las}}{32\pi * k * \alpha * (T - T_0)} \quad (13)$$

Therefore, $DA \rightarrow BLI$ limit conditions on the $P-u_{las}$ process map are expressed when:

$$P * u_{las} < \frac{48\pi^3 * k * \alpha * (T - T_0)}{A * e} \quad (14)$$

LoF border definition: Two limit conditions are identified to prevent the occurrence of LoF defects: the melt pool penetration within the printed material (D in Fig. 4) must be at least 15 μm deep [47] to guarantee good layer adhesion. The tracks of the *layer n* should at least join each other at the $n/n-1$ layer interface (as illustrated in Fig. 4), that is to say, η should be lower than or equal to W . Considering the width fluctuation of the molten track, a safety coefficient of 0.8 is recommended, where $\eta = 0.8 * W$. Among the different analytical models available in the literature, the one proposed by Tran and Lo [47] is probably the most relevant to identify the *LoF* border. Their model (T-L model) indeed considers the powder's absorption and its dependency on the layer thickness. Contrary

to the *KH* and *BLI* borders where the material is already in a liquid state, the *LoF* \rightarrow *DA* change involves the transition from powder to molten state.

Tran and Lo show in their work [48] that their model can provide a good prediction of the width and depth of the melt pool - at least for a thermal conduction regime, which is the case for conditions nearly above the *LoF* border. The T-L model is based exclusively on material properties (at powder and liquid states) and laser properties such as beam diameter σ and wavelength. For the sake of simplicity, the effect of σ on the *LoF* domain is not represented in Fig. 3.

For a defined D_{limit} (15 μm) and σ , the border *LoF* \rightarrow *DA* varied with h , given that the penetration of the melt pool depends on the absorption of the powder, and so the layer thickness. Because the absorption of the powder layer gets higher and the D diminishes with the increase of the h , the *LoF* \rightarrow *DA* transition is reached for higher P and lower u_{las} when h is increased, as illustrated in Fig. 3. Because *KH* and *BLI* borders are not h -dependent, an increase in the layer thickness leads to the diminution of the *DA* area.

Selection of h , u_{las} and η :

The material properties, the laser spot diameter, and meaningful limit conditions are thus enough to provide the *KH* and *BLI* borders. The calculation of the *LoF* border, which is required for further identification of the *DA* and valid combinations of $[P, u_{\text{las}}, \eta]$, leads to choosing the powder layer thickness, which is, as such, unknown.

Nevertheless, relevant values of h , u_{las} and η can be obtained when the following strategy is carried out: by selecting the layer thickness value (referred later as h_{limit}) for which the *KH*, the *BLI* and *LoF* borders intersect (see red dot in Fig 3; layer thickness = h_3 ; laser spot size = σ_1), *DA* is turned to the minimum space possible enabling the highest scanning speed ($u_{\text{las_limit}}$) for the printing of a dense product. Knowing $u_{\text{las_limit}}$, both the limit power P_{limit} and the limit melt pool width, and therefore η_{limit} , are known. This configuration provides an ideal scan time t_{scan} as both the layer thickness h and the hatch distance η reach their highest theoretical values, and because the fastest laser speed u_{las} from the dense area *DA* is selected. Such an approach is important for both customers and producers, because a high layer thickness and high scanning speed lead to a lower printing time [49] and therefore to a lower build cost.

From the quality's perspective, however, this approach brings a risk of having insufficient adhesion of layers because the printing conditions are close to the *LoF* border. Moreover, the layer could show *KH* porosity because small process deviations could easily lead the printing parameters to fall into the *KH* domain. Beyond these considerations, an analytical model providing an accurate melt pool width W for such printing conditions must be found.

Because the surface roughness of the printed part is known to be affected by h [49], this PMI could be used to select a proper layer thickness. However, the surface roughness depends likewise on other parameters, such as the powder distribution, the laser power, or the scanning strategy [50], and no linear correlation can be expected between it and h . It can be however expected that low h is a necessary condition to obtain a low surface roughness.

A more practical approach and valid alternative for selecting the critical parameters h , u_{las} and η is found with the volumetric Energy Density ED . This parameter represents the ideal energy provided per unit volume of material during the printing. ED is one of the driving keys to target high material density and is often used by researchers and engineers during the parameter design phase because it combines process parameters having an important effect on the quality of a printed part (see equation 15).

$$ED = \frac{P}{\eta * h * u_{\text{las}}} \quad (15)$$

The authors are well aware of the dubious character of ED [43]. However, the definition of the *KH*,

BLI, and *LoF* borders as previously described (see equations 11, 14 and *LoF* border defined with h_{limit}) enables the identification of a value range of P and u_{las} belonging to *DA*. Considering them in equation (15) should give a reliable trait to *ED* by preventing the use of $[P, u_{las}]$ combinations belonging to *KH*, *BLI* or *LoF* areas. The study [51] illustrate in Fig 7. how combinations of $[P, u_{las}]$ belonging to the *BLI* domain and combined with a relevant *ED* can lead to unstable printing conditions.

Therefore, it is suggested that a trustable average energy density ED_{avg} can be obtained by performing a statistical analysis of the literature on the *ED* values related to dense parts (>99%) of a dedicated material when the *DA* is considered. Out of ED_{avg} and P_{limit} , the build rate, $B_{rate} = \frac{P_{limit}}{ED_{avg}} = \eta_{avg} * h_{avg} * u_{las_limit}$ can be obtained.

Following this method, a reasonable $t_{scan,i}$ can be calculated simply with the volume of the raw part i , the printed material information, the identification of ED_{avg} and eventually the roughness. Because the type of material to be printed is systematically requested on the technical customer interface, a service provider can evaluate a scan time $t_{scan,i}$ already for a FQL 4, where V_i is provided, as long as ED_{avg} can be obtained from the literature. Scan time $t_{scan,i}$ evaluation with this method can be done at FQL 1 if a part allowance is assumed.

2.2.2 Calculation of $t_{scan,structure\ i}$

We assume that the process parameters used for printing the support structure are similar to the ones used for the product. The $t_{scan_structure}$ is calculated out of the equation (10) with the volume of the support structure.

2.2.3 Calculation of $t_{coating}$

$t_{coating}$ is expressed as $t_{coatinglayer} * n_{max}$, where $t_{coatinglayer}$ is the time required to spread one layer of powder, and n_{max} is the number of layers needed to print the highest part of a batch. This last term is obtained by dividing h_{max} by h . The first term is constant and machine-dependent. As shown before, our method provides decision-making factors to evaluate h . Thus, an ideal n_{max} can be calculated if h_{limit} is considered. A more conservative n_{max} value can be assessed through an exhaustive literature survey.

2.2.4 Calculation of t_{delay}

t_{delay} is related in the literature to $f * \frac{V_{bb,i}}{V_i}$, where f is a factor varying between 0 to 1 and V_{bb} is the bonding box's volume of the part i . The factor f reflects the variation of the unscanned areas along the build direction, and is empirically determined [3, 52–54], which brings subjective deviation to $C_{build,i}$. Moreover, the time t_{delay} depends on parameters such as the jump speed $u_{jump\ las}$ or the scanning strategy, which are not completely provided by data following a 3D master approach. We decided therefore to not include this term in our calculation model of $C_{build,i}$.

2.3 Closing the Gap between Present and Ideal Situation Regarding Models and PMI

The cost assessment methods proposed above by the authors rely mostly on PMI (ideally Formal Quality Level 7 of Table 1) and are therefore only viable if the customer thoroughly delivers them according to the 3D master approach. However, as previously mentioned, the industry has not yet adopted PMI and 3D master standards, at least for what concerns 3D printed parts [13].

Needing to close the gap between the present situation and 3D master method, we propose a short description of our AI-based tool, which aims to enable the transfer from the formal quality level 2 to level 3 as well as level 6 to 7.

Following three steps, our AI-based tool automatically maps PMI from a rasterized 2D technical drawing into a 3D STEP model. First, PMI elements are detected and mapped to their associated 2D part elements in each projection inside a technical drawing (step 1 in Fig. 5, H7 is mapped to the drill circle). Then, the (rasterized) projection(s) from the technical drawings are mapped to new (vectorized) projections of the 3D STEP model (step 2 in Fig. 5). Finally, we map the 2D element of the new projections to their corresponding 3D elements in the STEP model (step 3 in Fig. 5). Proceeding so, each PMI element from a 2D drawing is associated to its 3D element in the 3D model file.

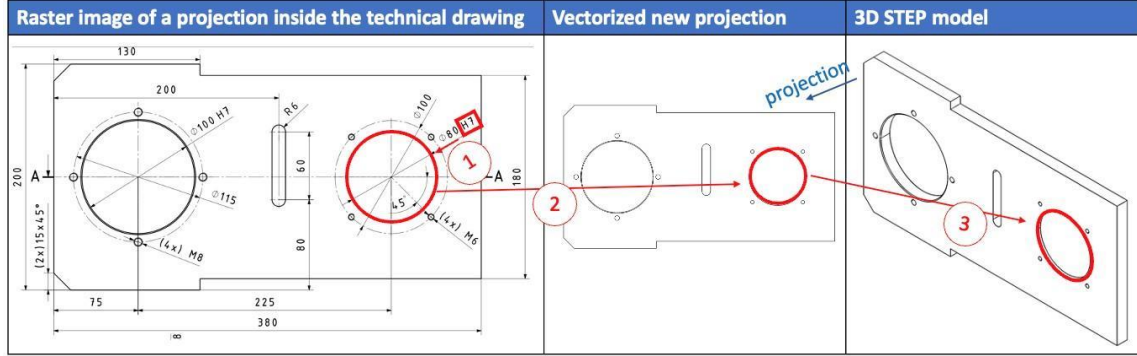


Fig. 5: main steps of the PMI generation supported by AI

More specifically, the first step is carried out using AI. A transformer network [55] is trained to transcribe a raster image to instructions that describe the image's content. Those instructions are the part elements (like the part's outline or drill holes), help elements (like arrows), PMI elements like tolerances), and their semantic connections. Then, the closest part element is heuristically identified for each PMI element using the semantic connections and help elements. The transformer network is trained end-to-end on synthetic data and projections of actual parts [56]. The second step is solvable by a heuristic algorithm matching the part element instructions with the corresponding new projection elements. The third step is primarily an engineering task using the fact that a STEP file is a 3D vector graphic (called a scene graph). The new projection is created using the hidden-line-removal algorithm [57], during which each responsible 3D element causing the specific 2D element is stored.

The ongoing work with our AI-based method provides a solution to generate PMI from conventional 2D and 3D files. Therefore, our methods proposed in Section 2 are realistic approaches.

3. Results of the t_{scan} Calculation Strategy, the Cost Model, and the KPI

Results of the calculation strategy to estimate t_{scan} and B_{rate}

The validation of our method to calculate t_{scan} (section 2.2.1) was done for the material Ti6Al4V by comparing the actual build rate B_{Arate} to the evaluated build rate B_{Erate} .

The KH and BLI borders, shown in Fig. 6, were calculated according to equations (11) and (14). Following our approach, the P_{limit} was identified to be the power for which these two borders intersect.

The average value of the laser spot size collected through the literature review ($\sigma_{avg}=88 \mu m$), as well as the maximum value $\sigma_{max}=220 \mu m$, were considered to illustrate the effect of σ on setting of the KH border. Therefore, two P_{limit} ($P_{limit@ \sigma_{avg}}$ and $P_{limit@ \sigma_{max}}$) are taken (see Fig. 6 and Table 2) for the

calculation of B_{Erate} . The material data was taken in [58].

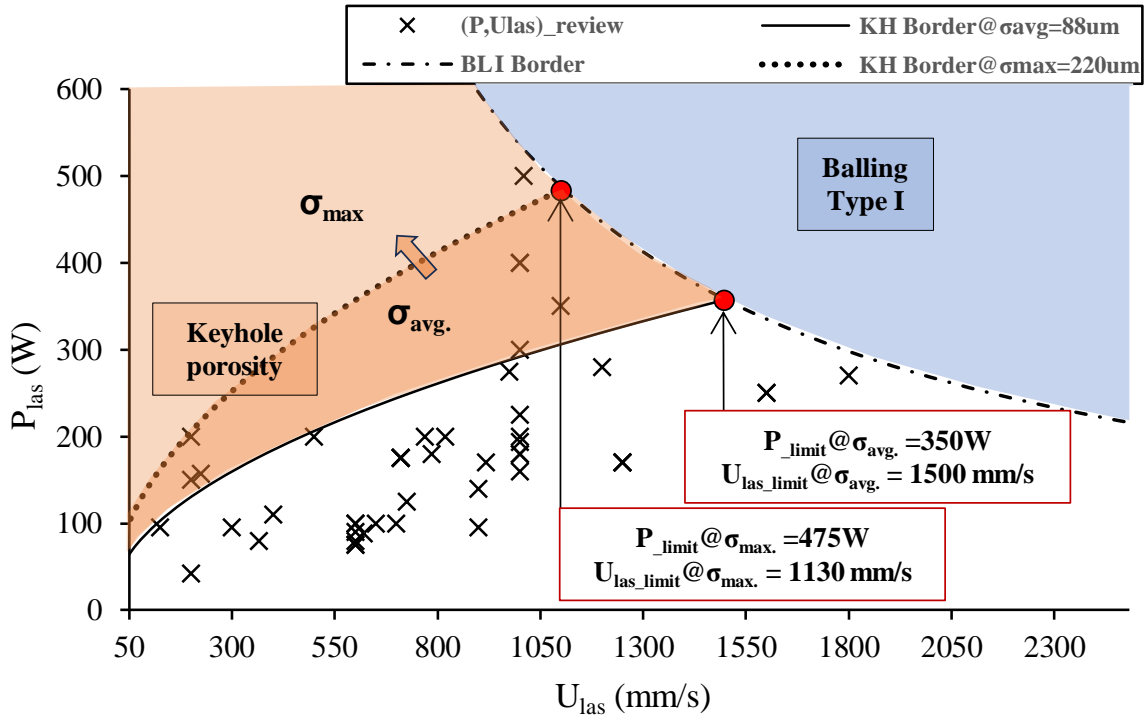


Fig. 6: Processing Map with KH and BLI borders for a Ti6Al4V material

Printing parameters data were collected from more than 40 works (see Table 2 of [59]), and the energy densities were calculated from values for which dense parts ($>99\%$) were obtained. The ED distribution, presented in Fig. 7, can be described with at least two normal distributions. The mean value of the population having the highest frequency was considered for ED_{avg} .

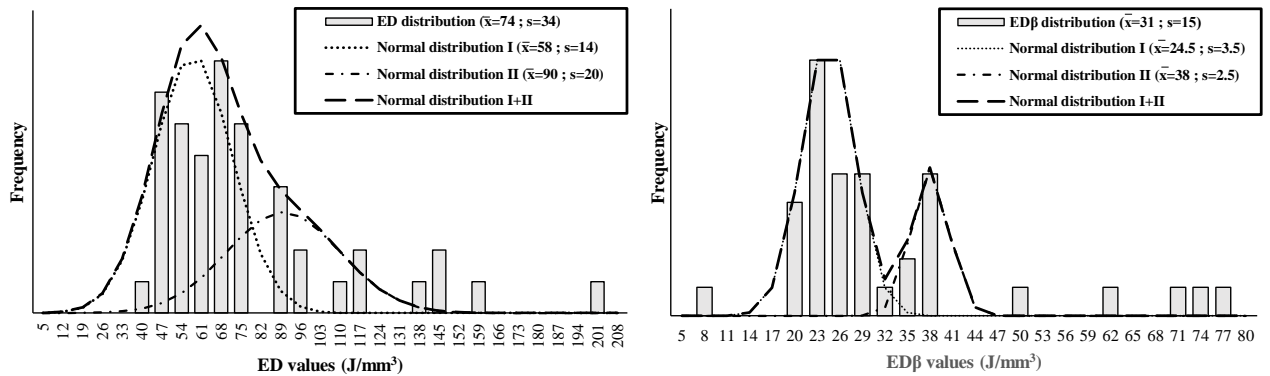


Fig. 7: ED and ED_{β} distribution for dense Ti6Al4V printed parts

ED_{avg} , $P_{limit@\sigma_{avg}}$ and $P_{limit@\sigma_{max}}$, B_{Arate} collected in the literature and the related B_{Erate} are gathered in Table 2.

The mean value of reviewed laser powers ($P_{avg_review} = 188$ W) was also considered, and the related estimated build rate B_{Erate} was also compared with the actual average build rate B_{Arate} . Finally, a B_{Erate} was also calculated in regard to our own printer Renishaw AM250, and the maximal laser power

($P_{max_AM250} = 200$ W) was taken. For information, the laser spot size of the Renishaw AM 250 is 80 μm .

Table 2: Comparison of B_{Erate} and B_{Arate} for different $P@σ$

$ED_{avg} = 58 \text{ J/mm}^3$				
	$P_{limit}@σ_{avg}$: 350 W@88μm	$P_{limit}@σ_{max}$: 475 W@220μm	P_{avg_review}: 188 W	$P_{max_AM250}@σ_{80}$: 200W@80μm
$B_{Arate} (\text{mm}^3.\text{s}^{-1})$	<i>B_{Arate} from the reviewed paper (mean value)</i> 2.9			<i>Intern optimized B_{Arate}</i> 3.6
$B_{Erate} (\text{mm}^3.\text{s}^{-1})$	6.0	8.2	3.2	3.4
Relative Deviation $\frac{ B_{Erate}-B_{Arate} }{B_{Arate}}$	107%	182%	10%	5.6%

Results of the model to estimate C_{Ebuild}

20 parts having various geometry complexity, different V_{bb}/V ratios, and different materials (1.2709, 1.4404, Inconel 718, Ti6Al4V) were produced with a Renishaw AM250 in our printing center. The printing parameters were internally optimized for each condition to reach a density above 99.0%. The estimated build cost $C_{Ebuild,i}$ obtained from our model (described in Section 2.2) was compared to the actual build cost $C_{Abuild,i}$. The results are presented in Table 3:

Table 3: Comparison between $C_{Ebuild,i}$ and $C_{Abuild,i}$

Part	1	2	3	4	5	6	7	8	9	10
$C_{Abuild,i} (\text{€})$	151.8	19.9	180.1	1285.8	829.8	27.5	275.0	38.3	152.2	132.0
$C_{Ebuild,i} (\text{€})$	149.2	19.2	186.1	1123.8	733.8	27.5	246.2	36.8	146.9	158.5
Relative Deviation $\frac{ C_{Ebuild,i} - C_{Abuild,i} }{C_{Abuild,i}}$	1.8%	3.6%	3.3%	12.6%	11.6%	0.0%	10.5%	3.9%	3.5%	20.1%

Part	11	12	13	14	15	16	17	18	19	20
$C_{Abuild,i} (\text{€})$	11.0	1345.9	1473.0	639.9	1134.7	1467.8	270.5	3493.4	1951.9	593.5
$C_{Ebuild,i} (\text{€})$	11.3	1200.1	1431.0	633.9	1164.7	1497.8	265.7	3676.4	2083.9	551.5
Relative Deviation $\frac{ C_{Ebuild,i} - C_{Abuild,i} }{C_{Abuild,i}}$	3.3%	10.9%	2.9%	0.9%	2.6%	2.0%	1.8%	5.2%	6.8%	7.1%

Relevance of the KPI to assess the formal quality level FQL

The calculation of the performance index was based on $C_{build,i}$. 13 metal AM models with a data set corresponding to formal quality level 7 were created. The build cost at level 3 (C_{Ebuild,i_level3}) was computed assuming that an offset of 0.5 mm over 20% of the raw part surface is needed for allowance. The real build costs, the estimated build costs, and the KPI for FQL 3 and FQL 7 are gathered in Table 4:

Table 4: Comparison between $C_{E\text{build},i}$ and $C_{A\text{build},i}$ for Formal Quality levels 3 and 7

Part	1	2	3	4	5	6	7	8	9	10
$C_{A\text{build},i}$ (€)	593.7	372.3	176.4	2280.2	135.5	348.4	1032.7	14.0	160.6	110.5
$C_{E\text{Build},i_level3}$ (€)	543.6	334.2	109.5	1739.0	117.4	305.7	931.8	16.3	165.0	86.5
$C_{E\text{Build},i_level7}$ (€)	644.8	383.4	154.8	2196.9	130.3	338.3	1021.9	14.4	166.9	121.8

Part	11	12	13	KPI_level3		KPI_level7
$C_{A\text{build},i}$ (€)	7.1	94.2	134.4			
$C_{E\text{Build},i_level3}$ (€)	7.0	78.8	125.9	17.5%		6.2%
$C_{E\text{Build},i_level7}$ (€)	7.2	101.4	135.5			

4. Discussion and validation of the t_{scan} Calculation Strategy, the Cost Model, and the KPI

Discussion and validation of the calculation strategy to estimate t_{scan} & B_{rate}

The two B_{Erate} calculated with the maximum laser power of our printing machine ($P_{\text{max_AM250}} = 200$ W) and with the average laser power from the literature review ($P_{\text{avg_review}} = 188$ W) show a good correlation with the actual results, with a relative deviation of 5.6% and 10% respectively.

On the contrary, the two theoretical build rates B_{Erate} calculated with $P_{\text{limit}@}\sigma_{\text{avg}}$ and $P_{\text{limit}@}\sigma_{\text{max}}$ are 2 to 2.8 times higher than the average B_{Arate} value obtained from the literature ($2.9 \text{ mm}^3 \cdot \text{s}^{-1}$).

These discrepancies illustrate on the one hand the importance for a service provider to consider the machine's technical limitations like the maximal laser power and the laser spot size because they play a role in the definition of the P_{limit} .

On the other hand, the difference between the estimated and actual build rates can be explained by the high discrepancy in ED values leading to high densities (>99%), as illustrated for example in Fig.7.

To address this issue, Oliveira et al.[43] to have suggested to modify the ED calculation by a introducing a dimensionless factor β , expressed as the ratio of the beam diameter over the powder size distribution. This new definition of the Energy Density, referred as ED_{β} , is relevant from the theoretical point of view because these two parameters contribute to the KH border (equation (11)) and the LoF border definition. Despite this approach, the ED_{β} values distribution (see Fig. 7) shows a high dispersion with a standard deviation (s) close to 50% of the mean value, which is similar to what is observed for the ED population. The factor β is therefore not efficient in reducing the ED values discrepancy.

Considering the reviewed studies for which the ED is higher than $ED_{\text{avg}} + 3s$, (referred as S_{+3s}), around 70% of them (referred as $S_{+3s_70\%}$) are carried out with a $[P, u_{\text{las}}, \eta]$ combination preventing the KH , BLI and LoF events from occurring. The high ED value is due for 80% of the $S_{+3s_70\%}$ to the setting of a low layer thickness ($\sim 20 \mu\text{m}$), showing that the printing time was of minor concern for the authors having conducted these studies. The other 20% of the $S_{+3s_70\%}$ studies show a narrow hatch distance, which leads to high ED and low build rate ($0.8 \text{ mm}^3 \cdot \text{s}^{-1}$). Finally, 30% of S_{+3s} are working with both high P/u_{las} and high layer thicknesses, which might bring the printing conditions close to a mixed regime of KH and LoF .

According to these observations, the negligence of the cost factor mostly explains the high dispersion of the ED values, as 70% of S_{+3s} are working with a low η or h inducing a low t_{scan} . The ED distribution could be narrowed and shifted toward the lowest ED values by ensuring that the $[P, u_{las}, \eta, h]$ combinations belongs to DA , while the combinations $[u_{las}, \eta, h]$ are optimized to reach the highest build rate.

The theoretical build rate B_{Erate} obtained with our method can thus be regarded as a conservative optimal build rate. The maximal machine's laser power output and laser spot size must be included in the parameter selection approach.

Discussion and validation of the model to estimate C_{Ebuild}

An average relative deviation of 5.7% was reached, showing that our model based on equations (2) and (10) is relevant for evaluating the C_{Ebuild} .

The deviation can be explained by the assumptions made, i.e. the jumping time and the scanning laser strategy were not taken into account. Thus, a higher relative deviation could be expected for parts having high V_{bb}/V ratios, or for stripes and chess scanning strategies where large overlaps are programmed.

Discussion and relevance of the Key Performance Index

The KPI_{level3} value is calculated to be 11.3% higher than the KPI_{level7} , showing, in this case that this index can be a relevant tool to evaluate the formal quality level.

A higher difference between KPI_{level3} and KPI_{level7} could be expected if the total production cost instead of the C_{build} is considered. Indeed, the allowance assumption made for level 3 will at least affect the evaluation accuracy of the machining cost (belonging to C_{post}), thus increasing the KPI value.

The differences that might appear between the KPI values of levels 5/6 and those of levels 7/8 depend on human factors and are harder to quantify. Higher C_{prep} for FQL 5/6 can be caused by the time needed to interpret 2D drawings. If drawings are misread, all the cost types (C_{prep} , C_{build} , and C_{post}) can be affected at different and unpredictable scales. The standardization of the data for production to level 7 or 8 following a 3D master approach would prevent this type of misinterpretation.

5. Conclusion and Perspective

This contribution defines a new and promising KPI as a tool helping the service providers to evaluate the impact of customer's data quality level on the cost estimation of AM parts printed with a PBF-LB/M process.

It also addresses the assessment of a production cost even when data regarding the part to be printed are lacking. With a few machine specifications (laser power, laser beam spot diameter), the type of material and an ED_{avg} , a conservative optimal build rate can be calculated already for a FQL4. This build rate is used to calculate the C_{Ebuild} with a model that has shown a relative deviation lower than 10%.

Our approach can support both manufacturing service providers and producers in better evaluating the final cost of MAM parts at an early stage of the production process. The cost evaluation must also consider the effect of the batch composition, as it has been shown that a mixed-build job batch caused a reduction in the cost per part [18, 60].

Our future work will aim to identify analytical models providing more accurate melt pool size for the printing conditions $[P_{limit}, u_{las_limit}, h_{limit}]$ for which KH and LoF domains are close to each other. It would enable the calculation of the η_{limit} and an ideal ED_{limit} . This approach could also be used with

the P_{max} of the printing machine, to bring a more realistic build rate and ED .

Future works will also focus on our AI-based tool to improve its scalability. A machine-readable PMI would improve the cost calculation based on the manufacturing information, e.g. critical dimensions, tolerances, and surface roughnesses. Besides the strong inertia for adopting PMI widely, the current STEP standard (without PMI) reduces the accuracy of the cost evaluation. If semantic information can be read as values with an AI tool, some PMI of interest are referenced in a non-semantic manner. These data are therefore not easily machine-readable, and a related interpreter add-in would be required.

References

1. Parenti, P., Puccio, D., Semeraro, Q., Colosimo, B.M.: A techno-economic approach for decision-making in metal additive manufacturing: metal extrusion versus single and multiple laser powder bed fusion. *Prog Addit Manuf.* 9, 185–210 (2024). <https://doi.org/10.1007/s40964-023-00442-7>
2. Mandolini, M., Sartini, M., Favi, C., Germani, M.: Cost Sensitivity Analysis for Laser Powder Bed Fusion. *Proc. Des. Soc.* 2, 1411–1420 (2022). <https://doi.org/10.1017/pds.2022.143>
3. Gibson, I., Rosen, D.W., Stucker, B.: *Additive Manufacturing Technologies: Rapid Prototyping to Direct Digital Manufacturing*. Springer US, Boston, MA (2010)
4. Mai, J., Zhang, L., Tao, F., Ren, L.: Customized production based on distributed 3D printing services in cloud manufacturing. *Int J Adv Manuf Technol.* 84, 71–83 (2016). <https://doi.org/10.1007/s00170-015-7871-y>
5. Cao, Q., Bai, Y., Zhang, J., Shi, Z., Fuh, J.Y.H., Wang, H.: Removability of 316L stainless steel cone and block support structures fabricated by Selective Laser Melting (SLM). *Materials & Design.* 191, 108691 (2020). <https://doi.org/10.1016/j.matdes.2020.108691>
6. Kitsios, V., Haslauer, R.: *3D-Master: Zeichnungslose Produktbeschreibung mit CATIA V5*. Springer Fachmedien, Wiesbaden (2014)
7. Groß, T.: Product Manufacturing Information (PMI). In: Groß, T. (ed.) *Technische Produktdokumentation: Detaillierungsfunktionen mit Siemens NX*. pp. 21–35. Springer Fachmedien, Wiesbaden (2020)
8. Wünsch, A., Pilz, F.: *Siemens NX für Einsteiger – kurz und bündig*. Springer Fachmedien, Wiesbaden (2020)
9. Blaschke, P., Wünsch, A.: *Siemens NX für Fortgeschrittene – kurz und bündig*. Springer Fachmedien, Wiesbaden (2023)
10. Kitsios, V.: *Ihre Produktentwicklung digitalisieren: In einfachen Schritten den Grundstein für die digitale Transformation legen*. Springer Fachmedien, Wiesbaden (2021)
11. *Advanced Design and Manufacturing Based on STEP*.
12. Feeney, A.B., Frechette, S.P., Srinivasan, V.: A Portrait of an ISO STEP Tolerancing Standard as an Enabler of Smart Manufacturing Systems. *Journal of Computing and Information Science in Engineering.* 15, 021001 (2015). <https://doi.org/10.1115/1.4029050>
13. Schmid, D.: Design And Release Process For AM Parts. Presented at the PLM Conference , Montréal July 10 (2023)
14. Real Time Manufacturing Services, <https://www.bossard.com/global-en/product-solutions/real-time-manufacturing-services/>
15. TICC - Graphical interactive time and cost calculation software, <https://www.r-u-b.de/en/ticc/>
16. Witherell, P., Herron, J., Ameta, G.: Towards Annotations and Product Definitions for Additive Manufacturing. *Procedia CIRP.* 43, 339–344 (2016). <https://doi.org/10.1016/j.procir.2016.01.198>
17. Baumers, M., Tuck, C., Wildman, R., Ashcroft, I., Rosamond, E., Hague, R.: Transparency Built-in: Energy Consumption and Cost Estimation for Additive Manufacturing. *J of Industrial Ecology.* 17, 418–431 (2013). <https://doi.org/10.1111/j.1530-9290.2012.00512.x>
18. Rickenbacher, L., Spierings, A., Wegener, K.: An integrated cost-model for selective laser melting (SLM). *Rapid Prototyping Journal.* 19, 208–214 (2013). <https://doi.org/10.1108/13552541311312201>
19. Alexander, P., Allen, S., Dutta, D.: Part orientation and build cost determination in layered manufacturing. *Computer-Aided Design.* 30, 343–356 (1998). [https://doi.org/10.1016/S0010-4485\(97\)00083-3](https://doi.org/10.1016/S0010-4485(97)00083-3)

20. Hopkinson, N., Dicknes, P.: Analysis of rapid manufacturing—using layer manufacturing processes for production. *Proceedings of the Institution of Mechanical Engineers, Part C: Journal of Mechanical Engineering Science*. 217, 31–39 (2003). <https://doi.org/10.1243/095440603762554596>
21. Kadir, A.Z.A., Yusof, Y., Wahab, M.S.: Additive manufacturing cost estimation models—a classification review. *Int J Adv Manuf Technol*. 107, 4033–4053 (2020). <https://doi.org/10.1007/s00170-020-05262-5>
22. Roth, M., Schaechtl, P., Giesert, A., Schleich, B., Wartzack, S.: Toward cost-efficient tolerancing of 3D-printed parts: a novel methodology for the development of tolerance-cost models for fused layer modeling. *Int J Adv Manuf Technol*. 119, 2461–2478 (2022). <https://doi.org/10.1007/s00170-021-08488-z>
23. Budinoff, H.D., Shafae, M.: Connecting part geometry and cost for metal powder bed fusion. *Int J Adv Manuf Technol*. 121, 6125–6136 (2022). <https://doi.org/10.1007/s00170-022-09688-x>
24. Kamps, T., Lutter-Guenther, M., Seidel, C., Gutowski, T., Reinhart, G.: Cost- and energy-efficient manufacture of gears by laser beam melting. *CIRP Journal of Manufacturing Science and Technology*. 21, 47–60 (2018). <https://doi.org/10.1016/j.cirpj.2018.01.002>
25. Faludi, J., Bayley, C., Bhogal, S., Iribarne, M.: Comparing environmental impacts of additive manufacturing vs traditional machining via life-cycle assessment. *Rapid Prototyping Journal*. 21, 14–33 (2015). <https://doi.org/10.1108/RPJ-07-2013-0067>
26. Dogea, R., Yan, X.T., Millar, R.: An extended cost analysis method for complex lightweight aircraft components manufactured with selective laser melting. *SN Appl. Sci*. 5, 182 (2023). <https://doi.org/10.1007/s42452-023-05382-z>
27. Toshev, R., Kolatsis, N., Shamzzuzoha, A., Helo, P.: The economics of additive manufacturing and topology optimisation – a case analysis of the electric scooter. *Journal of Engineering Design*. 34, 313–338 (2023). <https://doi.org/10.1080/09544828.2023.2205808>
28. Atzeni, E., Salmi, A.: Economics of additive manufacturing for end-usable metal parts. *Int J Adv Manuf Technol*. 62, 1147–1155 (2012). <https://doi.org/10.1007/s00170-011-3878-1>
29. Laureijs, R.E., Roca, J.B., Narra, S.P., Montgomery, C., Beuth, J.L., Fuchs, E.R.H.: Metal Additive Manufacturing: Cost Competitive Beyond Low Volumes. *Journal of Manufacturing Science and Engineering*. 139, 081010 (2017). <https://doi.org/10.1115/1.4035420>
30. Barclift, M., Joshi, S., Simpson, T., Dickman, C.: Cost Modeling and Depreciation for Reused Powder Feedstocks in Powder Bed Fusion Additive Manufacturing. *Solid Freeform Fabrication 2016*. 2007–2028 (2016)
31. Di, L., Yang, Y.: Cost Modeling and Evaluation of Direct Metal Laser Sintering with Integrated Dynamic Process Planning. *Sustainability*. 13, 319 (2020). <https://doi.org/10.3390/su13010319>
32. Colosimo, B.M., Cavalli, S., Grasso, M.: A cost model for the economic evaluation of in-situ monitoring tools in metal additive manufacturing. *International Journal of Production Economics*. 223, 107532 (2020). <https://doi.org/10.1016/j.ijpe.2019.107532>
33. Ding, J., Baumers, M., Clark, E.A., Wildman, R.D.: The economics of additive manufacturing: Towards a general cost model including process failure. *International Journal of Production Economics*. 237, 108087 (2021). <https://doi.org/10.1016/j.ijpe.2021.108087>
34. Zhang, Y., Bernard, A., Valenzuela, J.M., Karunakaran, K.P.: Fast adaptive modeling method for build time estimation in Additive Manufacturing. *CIRP Journal of Manufacturing Science and Technology*. 10, 49–60 (2015). <https://doi.org/10.1016/j.cirpj.2015.05.003>
35. Mahadik, A., Masel, D.: Implementation of Additive Manufacturing Cost Estimation Tool (AMCET) Using Break-down Approach. *Procedia Manufacturing*. 17, 70–77 (2018). <https://doi.org/10.1016/j.promfg.2018.10.014>
36. Piili, H., Happonen, A., Väistö, T., Venkataramanan, V., Partanen, J., Salminen, A.: Cost Estimation of Laser Additive Manufacturing of Stainless Steel. *Physics Procedia*. 78, 388–396 (2015). <https://doi.org/10.1016/j.phpro.2015.11.053>
37. Lindemann, C., Jahnke, U., Moi, M., Koch, R.: Analyzing Product Lifecycle Costs for a Better Understanding of Cost Drivers in Additive Manufacturing. *Solid Freeform Fabrication 2012*. 177–188 (2012)
38. Salmi, A., Calignano, F., Galati, M., Atzeni, E.: An integrated design methodology for components produced by laser powder bed fusion (L-PBF) process. *Virtual and Physical Prototyping*. 13, 191–202 (2018). <https://doi.org/10.1080/17452759.2018.1442229>
39. STL files explained | Learn about the STL file format | Adobe, <https://www.adobe.com/creativecloud/file->

types/image/vector/stl-file.html

40. King, W.E., Barth, H.D., Castillo, V.M., Gallegos, G.F., Gibbs, J.W., Hahn, D.E., Kamath, C., Rubenchik, A.M.: Observation of keyhole-mode laser melting in laser powder-bed fusion additive manufacturing. *Journal of Materials Processing Technology*. 214, 2915–2925 (2014). <https://doi.org/10.1016/j.jmatprotec.2014.06.005>
41. Zhu, J.-N., Borisov, E., Liang, X., Farber, E., Hermans, M.J.M., Popovich, V.A.: Predictive analytical modelling and experimental validation of processing maps in additive manufacturing of nitinol alloys. *Additive Manufacturing*. 38, 101802 (2021). <https://doi.org/10.1016/j.addma.2020.101802>
42. Seede, R., Shoukr, D., Zhang, B., Whitt, A., Gibbons, S., Flater, P., Elwany, A., Arroyave, R., Karaman, I.: An ultra-high strength martensitic steel fabricated using selective laser melting additive manufacturing: Densification, microstructure, and mechanical properties. *Acta Materialia*. 186, 199–214 (2020). <https://doi.org/10.1016/j.actamat.2019.12.037>
43. Oliveira, J.P., Santos, T.G., Miranda, R.M.: Revisiting fundamental welding concepts to improve additive manufacturing: From theory to practice. *Progress in Materials Science*. 107, 100590 (2020). <https://doi.org/10.1016/j.pmatsci.2019.100590>
44. Eagar, T.V.: Temperature Fields Produced by Traveling Distributed Heat Sources.
45. Cunningham, R., Zhao, C., Parab, N., Kantzos, C., Pauza, J., Fezzaa, K., Sun, T., Rollett, A.D.: Keyhole threshold and morphology in laser melting revealed by ultrahigh-speed x-ray imaging. *Science*. 363, 849–852 (2019). <https://doi.org/10.1126/science.aav4687>
46. Poirier, D.R., Geiger, G.H.: *Transport Phenomena in Materials Processing*. Springer (2016)
47. Tran, H.-C., Lo, Y.-L.: Systematic approach for determining optimal processing parameters to produce parts with high density in selective laser melting process. *Int J Adv Manuf Technol*. 105, 4443–4460 (2019). <https://doi.org/10.1007/s00170-019-04517-0>
48. Tran, H.-C., Lo, Y.-L.: Heat transfer simulations of selective laser melting process based on volumetric heat source with powder size consideration. *Journal of Materials Processing Technology*. 255, 411–425 (2018). <https://doi.org/10.1016/j.jmatprotec.2017.12.024>
49. Shi, X., Yan, C., Feng, W., Zhang, Y., Leng, Z.: Effect of high layer thickness on surface quality and defect behavior of Ti-6Al-4V fabricated by selective laser melting. *Optics & Laser Technology*. 132, 106471 (2020). <https://doi.org/10.1016/j.optlastec.2020.106471>
50. M., K., T., T.: Surface Quality Research for Selective Laser Melting of Ti-6al-4v Alloy. *Archives of Metallurgy and Materials*. 61, 1291–1296 (2016). <https://doi.org/10.1515/amm-2016-0213>
51. Scipioni Bertoli, U., Wolfer, A.J., Matthews, M.J., Delplanque, J.-P.R., Schoenung, J.M.: On the limitations of Volumetric Energy Density as a design parameter for Selective Laser Melting. *Materials & Design*. 113, 331–340 (2017). <https://doi.org/10.1016/j.matdes.2016.10.037>
52. Pham, D.T., Wang, X.: Prediction and reduction of build times for the selective laser sintering process. *Proceedings of the Institution of Mechanical Engineers, Part B: Journal of Engineering Manufacture*. 214, 425–430 (2000). <https://doi.org/10.1243/0954405001517739>
53. Ruffo, M., Tuck, C., Hague, R.: Empirical laser sintering time estimator for Duraform PA. *International Journal of Production Research*. 44, 5131–5146 (2006). <https://doi.org/10.1080/00207540600622522>
54. Wilson, J.O., Rosen, D.: Selection for Rapid Manufacturing Under Epistemic Uncertainty, <http://proceedings.asmedigitalcollection.asme.org/proceeding.aspx?articleid=1588511>, (2005)
55. Vaswani, A., Shazeer, N., Parmar, N., Uszkoreit, J., Jones, L., Gomez, A.N., Kaiser, L., Polosukhin, I.: Attention Is All You Need. ." *Advances in neural information processing systems*. 30, (2017). <https://doi.org/10.48550/arXiv.1706.03762>
56. Koch, S., Matveev, A., Jiang, Z., Williams, F., Artemov, A., Burnaev, E., Alexa, M., Zorin, D., Panozzo, D.: ABC: A Big CAD Model Dataset For Geometric Deep Learning. *Proceedings of the IEEE/CVF conference on computer vision and pattern recognition*. (2019). <https://doi.org/10.48550/arXiv.1812.06216>
57. Galimberti, R.: An algorithm for hidden line elimination. *Commun. ACM*. 12, 206–211 (1969). <https://doi.org/10.1145/362912.362921>
58. Bartsch, K., Herzog, D., Bossen, B., Emmelmann, C.: Material modeling of Ti–6Al–4V alloy processed by laser powder bed fusion for application in macro-scale process simulation. *Materials Science and Engineering: A*. 814, 141237 (2021). <https://doi.org/10.1016/j.msea.2021.141237>
59. Singla, A.K., Banerjee, M., Sharma, A., Singh, J., Bansal, A., Gupta, M.K., Khanna, N., Shahi, A.S., Goyal,

- D.K.: Selective laser melting of Ti6Al4V alloy: Process parameters, defects and post-treatments. *Journal of Manufacturing Processes*. 64, 161–187 (2021). <https://doi.org/10.1016/j.jmapro.2021.01.009>
60. Ruffo, M., Hague, R.: Cost estimation for rapid manufacturing ' simultaneous production of mixed components using laser sintering. *Proceedings of the Institution of Mechanical Engineers, Part B: Journal of Engineering Manufacture*. 221, 1585–1591 (2007). <https://doi.org/10.1243/09544054JEM894>